Ocean Engineering 235 (2021) 109055

Contents lists available at ScienceDirect

Ocean Engineering

journal homepage: www.elsevier.com/locate/oceaneng

Dynamic positioning of floating caissons based on the UKF filter under external perturbances induced by waves

Elías Revestido Herrero [a,*], Jose Ramon Llata [b], Esther Gonzalez-Sarabia [b], Francisco J. Velasco [a], Jose Joaquin Sainz [b], Alvaro Rodriguez-Luis [c], Sergio Fernandez-Ruano [c], Raul Guanche [c]

[a] Department of Electronic Technology, Systems Engineering and Automatic Control, University of Cantabria. E.T.S. de Náutica, C/ Gamazo 1- 39004 Santander (Cantabria), Spain

[b] Department of Electronic Technology, Systems Engineering and Automatic Control, University of Cantabria. E.T.S. de Ingenieros Industriales y de Telecomunicacion, Av. de los Castros s/n- 39005 Santander (Cantabria), Spain

[c] Environmental Hidraulics Institute, IH Cantabria, Universidad de Cantabria,c/ Isabel Torres n 15, Parque Cientifico y Tecnológico de Cantabria, 39011, Santander, Spain

ARTICLE INFO

Keywords:
Dynamic positioning
UKF
Classical controller
Control allocation

ABSTRACT

This paper presents a dynamic positioning control scheme for concrete caissons in an attempt to automate part of the manoeuvres which usually require a complex deploy of personnel and equipment for port infrastructures development. The aim of this paper is to propose a control scheme, which is able to provide a reduction in costs and an improvement in security for the dynamic positioning manoeuvres . To do so, a dual loop controller is developed and the unscented Kalman filter is applied for states and perturbances estimation. Furthermore, a control allocation algorithm is proposed based on anchoring lines and winches. Finally, some simulations are performed to verify the effectiveness of the proposed approach.

1. Introduction

Over the last few decades, the use of concrete caissons in port infrastructures has been developed greatly by means of the use of lightweight (floating) caissons and the improvements of the technology required for their manufacture (Cejuela et al., 2018). The process of port infrastructure construction involves different kinds of manoeuvres, one is the foundation manoeuvre. In the final phase of this manoeuvre, where the positioning and sinking of the caisson takes place, various teams take part in and must be coordinated to execute the positioning with accuracy. Currently, this manoeuvre is carried out by coordinating of both land-based (i.e. winches and windlasses) and marine equipment (i.e. tugs and auxiliary boats), and in most cases, the coordination is carried out by specialized personnel directly on the caisson. This manoeuvre is not performed without risk and accidents are common for many reasons: failure of coordination between teams, unexpected environmental loads, anchorage or malfunctioning of mooring lines, as well as human failure. Accidents may result in an inaccurate anchoring of the caisson, or even human damage, leading to economic losses and high risk for the personnel involved in the anchoring manoeuvres.

For all of the reasons cited above, any attempt to provide an automatic process for port infrastructure caisson construction can give as a result a significant reduction in costs and an improvement in security. In this paper, it is proposed a control scheme for the dynamic positioning (DP) of the caisson with the aim of decreasing costs and improving security. We focus on this DP manoeuvre, which requires a complex deploy of personnel and equipment as previously indicated. Within the vessels or floating structures DP design, the existing literature ranges from the application from PID and classical control techniques to modern techniques such as adaptive sliding, backsteeping, fuzzy or optimal control approaches (Xu and Liu, 2016; Xia et al., 2018; Fang and Lee, 2016; Xia et al., 2019; Zhao et al., 2019; Cheng-Du et al., 2013; Xu et al., 2014). A complete study of previous DP approaches can be found in Sorensen (2011) (and references therein). Furthermore, in the DP applications for vessels, different kind of methods have been applied for the states and the disturbances estimation including among others: the Kalman filter, the unscented Kalman filter (UKF) or particle filter (Chen et al., 2018; Jayasiri et al., 2017; Xu et al., 2013).

* Corresponding author.
E-mail addresses: revestidoe@unican.es (E.R. Herrero), llataj@unican.es (J.R. Llata), esther.gonzalezs@unican.es (E. Gonzalez-Sarabia), velascoj@unican.es (F.J. Velasco), josejoaquin.sainz@unican.es (J.J. Sainz), alvaro.rodriguezluis@unican.es (A. Rodriguez-Luis), sergio.fernandezruano@unican.es (S. Fernandez-Ruano), raul.guanche@unican.es (R. Guanche).
URLs: https://www.marinelabcantabria.unican.es (E.R. Herrero), https://www.marinelabcantabria.unican.es (J.R. Llata), https://www.marinelabcantabria.unican.es (F.J. Velasco).

https://doi.org/10.1016/j.oceaneng.2021.109055
Received 17 December 2020; Received in revised form 24 March 2021; Accepted 18 April 2021
Available online 23 June 2021

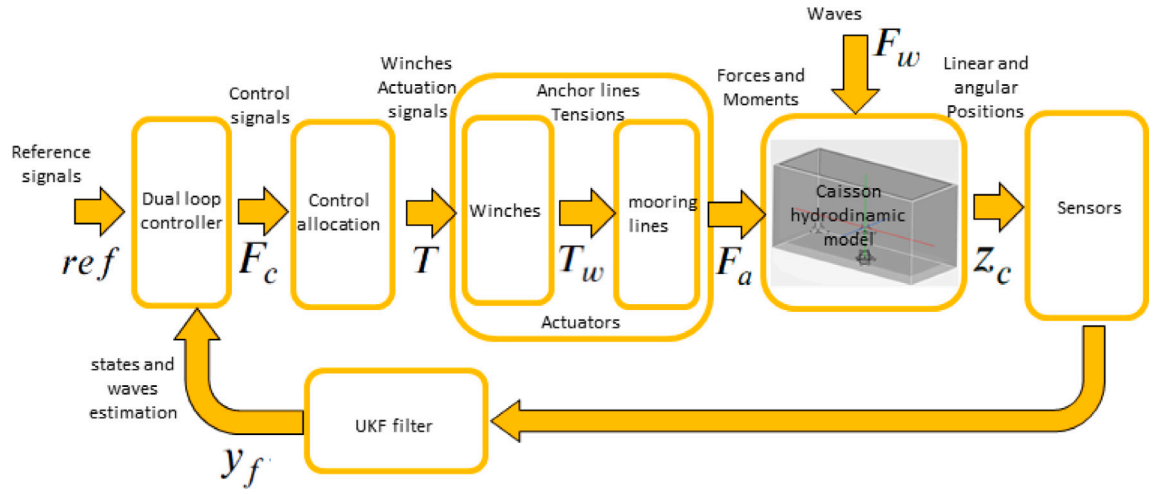

Fig. 1. Proposed control scheme for DP system (the variables pointed out in the figure are related to the sections below).

Table 1
Approximated model and controller Laplace transfer functions.

	Linear approximation	Controller (reference, integral term, Lead compensation term)	Parameter Criteria
Surge	$G_x = \frac{a_x}{s^2}$	$G_{rx} = \frac{K_{x_{ref}}}{(T_{x_{ref}}s+1)}$, $G_{ix} = \frac{1}{(T_{ix}s)}$, $G_{cx} = \frac{K_x(s+z_x)}{s+p_x}$	$p_x > 10z_x$
Sway	$G_y = \frac{a_y}{s^2}$	$G_{ry} = \frac{K_{y_{ref}}}{(T_{y_{ref}}s+1)}$, $G_{ry} = \frac{1}{(T_{iy}s)}$, $G_{cy} = \frac{K_y(s+z_y)}{s+p_y}$	$p_y > 10z_y$
Heading	$G_\psi = \frac{a_\psi}{s(b_\psi s+1)}$	$G_{r\psi} = \frac{K_{N_{ref}}}{(T_{N_{ref}}s+1)}$, $G_{r\psi} = \frac{1}{(T_{i\psi}s)}$, $G_{c\psi} = \frac{K_\psi(s+z_\psi)}{s+p_\psi}$	$p_\psi > 10z_\psi$

As far as the control allocation system is concerned, the control methods applied in the contributions cited above are based on thrusters. The control allocation methods for different types of thruster configurations can be found in Fossen and Johansen (2006) and Fossen and Perez (2009) for marine vehicles and in Johansen and Fossen (2013) a more general frame work for control allocation algorithms is presented. Moreover, DP control applications of moored vessels are also based on thrusters as it is shown in the contributions published by Aamo and Fossen (1999), Berntsen et al. (2008), Chen et al. (2013), where the mooring system is modeled by means of finite elements (Aamo and Fossen, 2001). Notwithstanding all the contributions cited above regarding to the DP control with an allocation system based on thrusters, specific contributions related to DP control of anchored caissons without thrusters are not found in the literature. In the allocation systems based on rotatable thrusters for marine vehicles, it is possible to control the thrust direction and its magnitude, this means that it is controlled the direction of the forces provoked in the vehicle. Furthermore, in the allocation systems with fixed thrusters, the thrust direction does not change with respect to the local coordinated system of the vehicle. However, in the allocation system for caissons of this work based on mooring lines, not only is the direction of the forces in the caisson not controlled but the direction of the forces also varies as a function of the relative position between the caisson and the anchoring points. This introduces instability to the system and makes it more difficult to control. [,belowfloat=15pt,abovecaption=13pt]

For all the reasons commented above, it is proposed a DP control scheme as shown in Fig. 1. A dual loop controller is developed with the UKF for states and disturbances estimation, which reduces errors in stationary state and provides stability to the caisson motion. Additionally, it is proposed an algorithm, easy to implement and computationally cheap, for the control allocation module of the DP control scheme. Our approach differs from the usual approach previously reported in the literature, whereby there are no thrusters and it is considered eight lines and winches distributed over the caisson as indicated in Appendix A.

Table 2
Weight distribution of the caisson.

	Value	Description
$m(kg)$	6366000	Total mass
$LenghtC(m)$	33.69	Length of the caisson.
$WidthC(m)$	19.6	Width of the caisson.
$HeightC(m)$	17.3	Height of the caisson.
$D_l(m)$	14	Depth of the mooring point, see Fig. 15.
$L_l(m)$	60	Length of the line, see Fig. 15.
$L_{c1}(m)$	$HeightC - D + D_l$	Height from the mooring point to the winche.
$L_{c2}(m)$	$\sqrt{L_l^2 - L_{c1}^2}$	Distance from the mooring point to the winche.
$C_{og}(m)$	−2.474	Position of the center of gravity in the Z axis.
$C_{ob}(m)$	−4,875	Position of the center of buoyancy in the Z axis.
D	9.75	Draft.
I_{xx} (kg m^2)	464290000	Inertia roll
I_{yy} (kg m^2)	865050000	Inertia pitch
I_{zz} (kg m^2)	865050000	Inertia yaw

- The application of the UKF filter for the estimation of anchored caisson states and waves perturbances.
- The application of a dual loop controller based on classical theory dynamic for DP control of anchored caissons without thrusters.
- The proposition of a control allocation system for anchored caissons based on eight mooring lines and winches without thrusters.

This paper is organized as follows. Section 2 discusses the dynamic model of the caisson with environmental disturbances and actuators models. Sections 3 and 4 develop the UKF-based nonlinear filter and the dual loop controller, respectively. Section 5 discusses the control allocation system. Section 6 presents de simulation results. The conclusions are drawn in Section 7.

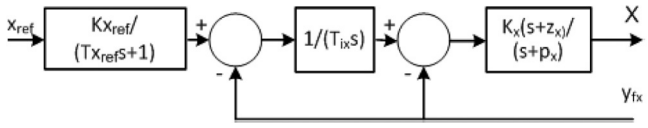

Fig. 2. Dual loop controller for the surge degree of freedom.

2. The model

2.1. Hydrodynamic model

The dynamic model of the caisson, object of study of this paper is represented by the following equation (Armesto et al., 2015):

$$(M + A_\infty)\ddot{z_c}(t) + \int K(t-\tau)\dot{z_c}(\tau)d\tau + Cz_c(t) = F_a(t) + F_w(t) \tag{1}$$

where $z_c(t) = [x, y, z, \phi, \theta, \psi]^T$ are the position and the Euler angles of the caisson, M is the mass of the caisson, A_∞ is the added mass at infinite frequency, K is the function of delay and fluid memory effects, C is the hydrostatic restoration coefficient and $F_a = [X_a, Y_a, Z_a, K_a, M_a, N_a]$ the actuators forces and moments and $F_w = [X_w, Y_w, Z_w, K_w, M_w, N_w]$ are the forces and moments induced by waves. The caisson's coordinate system is located in the center of gravity and is considered inertial, for more details of the caisson main features see Appendix A.

2.2. Waves model

Similar to the hydrodynamic model, the wave excitation model is also based in potential flow theory, broadly used in literature (Journee, 2001). Using a commercial Boundary Elements Method, the wave diffraction problem is solved, and the first order wave forces vector $F(\omega_i, \phi_k)$ is obtained for different wave angular frequencies ω_i and different wave headings ϕ_k. In an analogous way, the second order wave forces quadratic transfer function $QTF_{dif}(\omega_i, \omega_j, \phi_k)$ is obtained. Then, for any sea state represented with nC components of specific angular frequency ω_i, height H_i, heading ϕ_i and phase φ_i, the wave forces are computed in the time domain as shown in Eqs. (2) and (3).

$$F_{1st} = 0.5\sum_{i=1}^{nC} |F(\omega_i, \phi_i+\gamma)|H_i cos(-\omega_i t+\varphi_i+F(\omega_i, \phi_i+\gamma)+k_{x,i}x+k_{y,i}y) \tag{2}$$

$$\begin{aligned} F_{2nd} = 0.25\sum_{i=1}^{nC}\sum_{j=1}^{nC} H_i H_j |QTF_{dif}(\omega_i, \omega_j, 0.5(\phi_i+\phi_j)+\gamma)|\times \\ cos(-(\omega_i-\omega_j t+(\varphi_i-\varphi_j)+ \\ \widehat{QFT}_{dif}(\omega_i, \omega_j, 0.5(\phi_i+\phi_j)+\gamma)+(K_{x,i}-K_{x,j})x+(K_{y,i}-K_{y,j})y)) \end{aligned} \tag{3}$$

The total forces induced to the caisson are $F_w(t) = F_{1st} + F_{2nd}$.

2.3. Actuators model

The actuators of this work are made up by 8 turrets with 8 winches and 8 mooring lines, see Appendix A for details.

The winches are modeled by:

$$T_w = diag(K_{w1}, K_{w2}, K_{w3}, K_{w4}, K_{w5}, K_{w6}, K_{w7}, K_{w8})T \tag{4}$$

where $K_{wi}(i = 1 \dots 8)$ are the gains of the winches assembled in the caisson, and T are the tensions for each of the eight lines provided by the allocation system, see algorithm 1 in Section 5.

Moreover, the forces and moments components acting on the center of gravity of the caisson due to the winches are modeled by following the next procedure:

Firstly, it is calculated the position of the caisson referred to the inertial coordinate axe of the initial position of the caisson by doing:

$$P_{th} = T_{h1}T_{h2}T_h \tag{5}$$

where

$$\begin{aligned} T_{h1} &= \begin{bmatrix} c\psi c\theta & -s\psi c\phi + c\psi s\theta s\phi & s\psi s\phi + c\psi c\phi s\theta & x \\ s\theta & c\psi c\phi + s\phi s\theta s\phi & -c\psi s\phi + s\theta s\psi c\phi & y \\ s\theta & c\theta c\phi & c\theta c\phi & z \\ 0 & 0 & 0 & 1 \end{bmatrix} \\ T_{h2} &= \begin{bmatrix} 1 & 0 & 0 & 0 \\ 0 & 1 & 0 & 0 \\ 0 & 0 & 1 & D + C_{og} \\ 0 & 0 & 0 & 1 \end{bmatrix} \end{aligned} \tag{6}$$

$$T_h = \begin{bmatrix} & & & 1 \\ & & & 1 \\ & & & 1 \\ & P_T & & 1 \\ & & & 1 \\ & & & 1 \\ & & & 1 \end{bmatrix}^T \quad P_T = \begin{bmatrix} -(LengthC/2) & (WidthC/3) & -HeightC \\ (LengthC/2) & (WidthC/3) & -HeightC \\ -(LengthC/2) & -(WidthC/3) & -HeightC \\ (LengthC/2) & -(WidthC/3) & -HeightC \\ -(LengthC/4) & (WidthC/2) & -HeightC \\ (LengthC/4) & (WidthC/2) & -HeightC \\ -(LengthC/4) & -(WidthC/2) & -HeightC \\ (LengthC/4) & -(WidthC/2) & -HeightC \end{bmatrix} \tag{7}$$

where $s\cdot = sin(\cdot)$, $c\cdot = cos(\cdot)$ and P_T describes the position of the caisson's turrets refereed to the coordinate system of the caisson and T_{h2} includes features of the caisson, see Appendix A for the dimensions. Note that the matrix T_{h1} includes a rotation matrix so that the caisson rotates with respect to the center of gravity and the caisson's surge, sway and yaw components provided by the model defined in Eq. (1).

Undo the coordinate system change that was rotated with respect to the center of gravity.

$$P_{tnh} = T_{h3}P_{th} \tag{8}$$

where

$$T_{h3} = \begin{bmatrix} 1 & 0 & 0 & 0 \\ 0 & 1 & 0 & 0 \\ 0 & 0 & 1 & -(D + C_{og}) \\ 0 & 0 & 0 & 1 \end{bmatrix} \tag{9}$$

being D the draft of the caisson and C_{og} the position of the center of gravity in the Z axis, see Appendix A.

Calculate the new position of the mooring points with respect to the caisson's coordinate system:

$$P_{na} = M_1 M_2 P_a \tag{10}$$

where

$$M_1 = \begin{bmatrix} 1 & 0 & 0 & -x \\ 0 & 1 & 0 & -y \\ 0 & 0 & 1 & 0 \\ 0 & 0 & 0 & 1 \end{bmatrix} M_2 = \begin{bmatrix} cos(-\psi) & sin(-\psi) & 0 & 0 \\ sin(-\psi) & cos(-\psi) & 0 & 0 \\ 0 & 0 & 1 & 0 \\ 0 & 0 & 0 & 1 \end{bmatrix} \tag{11}$$

$$P_a = \begin{bmatrix} -(L_{c2} + LengthC/2) & (WidthC/3) & D_l - D \\ (Lc2 + LengthC/2) & (WidthC/3) & D_l - D \\ -(Lc2 + LengthC/2) & -(WidthC/3) & D_l - D \\ (Lc2 + LengthC/2) & -(WidthC/3) & D_l - D \\ -(LengthC/4) & +(L_{c2} + WidthC/2) & D_l - D \\ (LengthC/4) & +(L_{c2} + WidthC/2) & D_l - D \\ -(LengthC/4) & -(L_{c2} + WidthC/2) & D_l - D \\ (LengthC/4) & -(L_{c2} + WidthC/2) & D_l - D \end{bmatrix}^T \tag{12}$$

Note that the matrix P_a represents the position of the mooring points, see Appendix A and Table 2 for details on the dimensions.

Form the forces and moments director vectors from the caisson's coordinates system in each turret (eight turrets, see Appendix A for more details):

$$V_d = P_a - P_{tnh} \tag{13}$$

$$V_d = \frac{V_d}{\sqrt{V_d^T V_d}} \tag{14}$$

Calculate the force components in each line of the caisson:

$$F_l = [T_w \cdot [111]]^T \cdot V_d \tag{15}$$

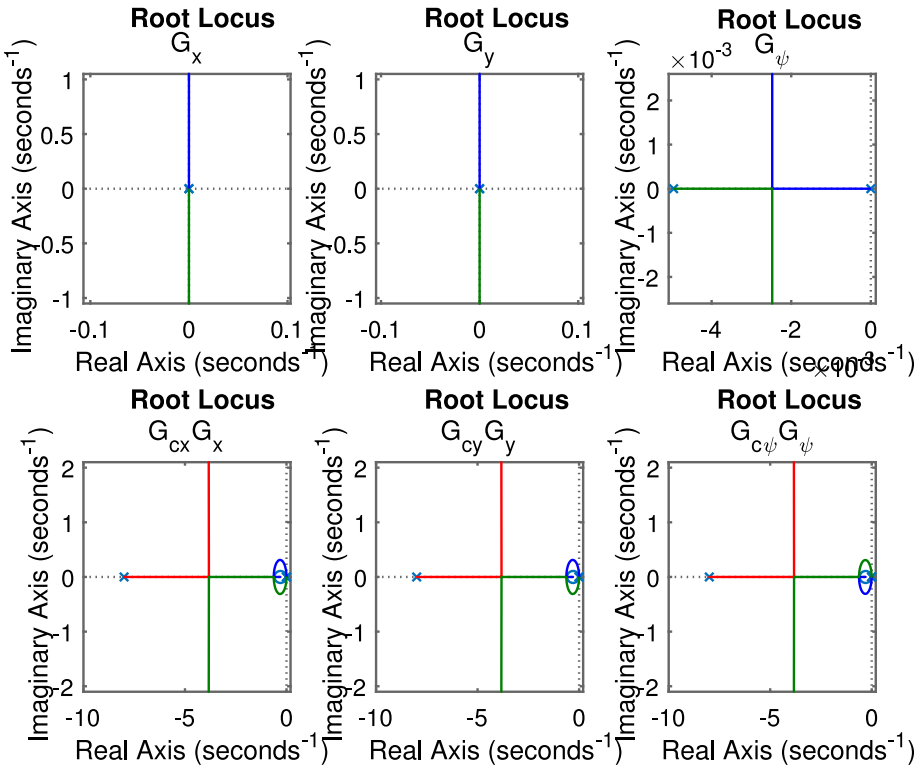

Fig. 3. Root locus of the linear approximations for the surge, sway and yaw degrees of freedom (top of the figure), linear approximations and lead compensation controller for surge, sway and yaw degrees of freedom (bottom of the figure).

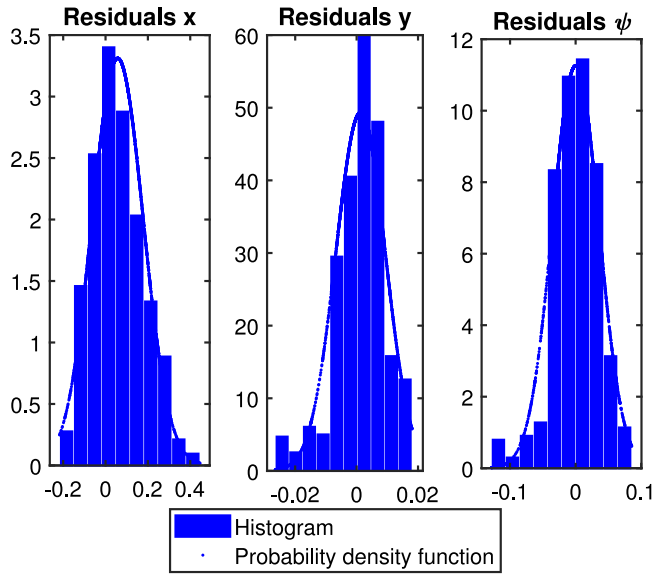

Fig. 4. Histogram and probability density function of the residuals obtained with the UKF filter.

Calculate the total forces:

$$F_t = \sum_{i=1}^{8} F_l(1..3, i) \tag{16}$$

In order to calculate the moments, form vectors from the center of gravity to each turret

$$M_c = P_{tnh} - \begin{bmatrix} 0 \\ 0 \\ -(D + C_{og}) \end{bmatrix} [11111111] \tag{17}$$

where the matrix P_{tnh} was previously calculated in Eq. (5).

Obtain the moments in each turret by doing the next cross product:

$$M_{lt} = M_c \times F_l \tag{18}$$

Finally, the total Moments are:

$$M_t = \sum_{i=1}^{8} M_{lt}(1..3, i) \tag{19}$$

Then, the forces and moments provoked by each of the turret in the center of gravity of the caisson is a vector defined by

$$F_a(t) = [F_t, -M_t] \tag{20}$$

Note that the forces and moments obtained in Eq. (20) are applied to Eq. (1).

3. Non linear filtering

The model in Eq. (1) is non linear, that is why the estimation of the states of the system constitutes a non linear filtering problem. This problem can be solved using the EKF, but it is well known that this filter is not robust with respect to the parameter uncertainty and can produce unstable filters if the assumptions of local linearity are violated (Sorenson, 1985; Uhlmann, 1992). To avoid these drawbacks, Julier and Uhlmann (1997) proposed the UKF, which has the following advantages: it can capture the mean and covariance with subsequent accuracy up to third order (Taylor series expansion) for any non-linearity and is robust to parameter uncertainty (Ristic et al., 2004).

In order to estimate the states of the model object of study of this paper (equation (1)) with the UKF filter, it is necessary to formulate an augmented discrete state space model as follows (Fossen and Perez, 2009):

$$\begin{bmatrix} x_{w(k+1)} \\ z_{c(k+1)} \end{bmatrix} = h \cdot \begin{bmatrix} A_{w_{6\times6}} \\ 0_{6\times6} \end{bmatrix} \begin{bmatrix} x_{w(k)} \\ z_{c(k)} \end{bmatrix} + \begin{bmatrix} x_{w(k)} \\ z_{c(k)} \end{bmatrix} + g_{(k)}(z_{c(k)}, F_{a(k)}) + w_{(k)} \tag{21}$$

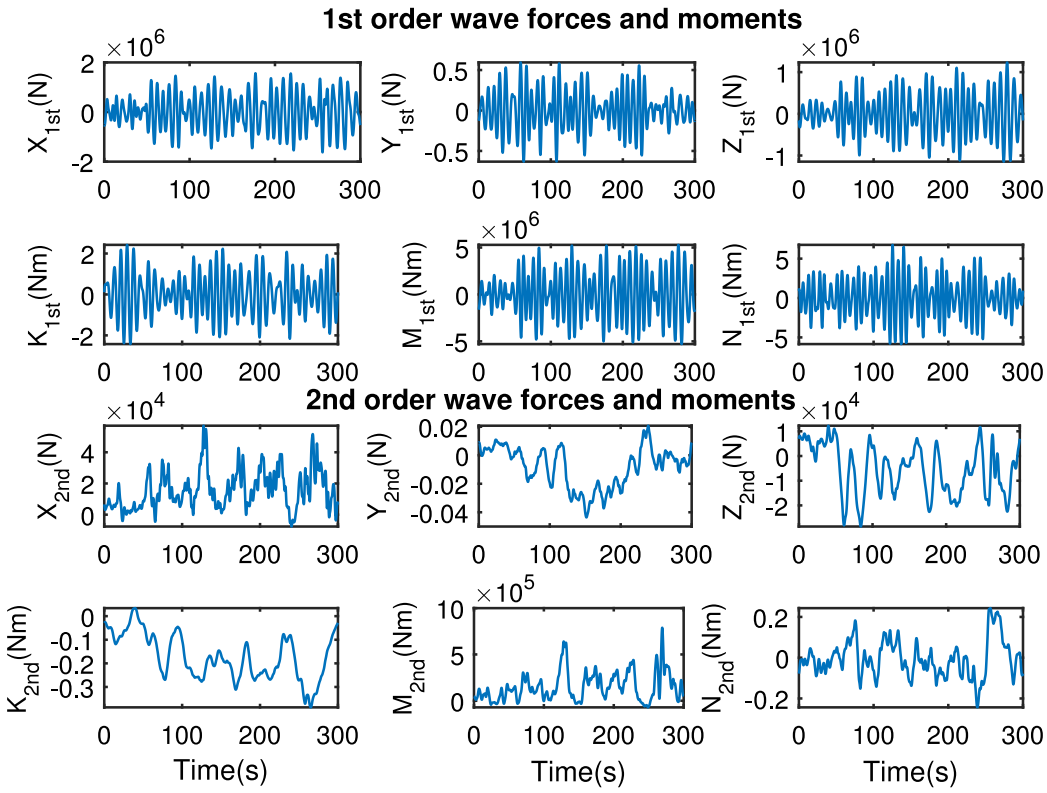

Fig. 5. First and second order wave forces and moments applied to the caisson.

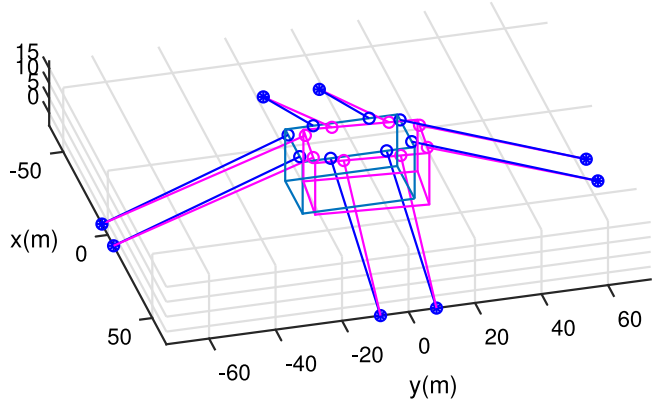

Fig. 6. Initial position of the caisson (x = 0, y = 0, blue) and final position (x = 4, y = 3 ,pink), 3GDL UKF control with waves. (For interpretation of the references to color in this figure legend, the reader is referred to the web version of this article.)

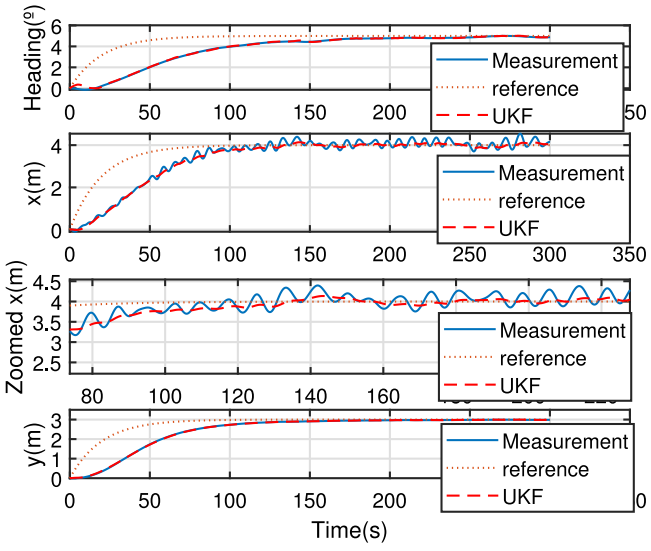

Fig. 7. 3GDL UKF control results with waves, position (x, y) and heading.

$$y_{f(k)} = \begin{bmatrix} 0_{6\times6} & 0_{6\times6} \\ C_{21_{6\times6}} & C_{22_{6\times6}} \end{bmatrix} \begin{bmatrix} x_{w(k)} \\ z_{c(k)} \end{bmatrix} + n_{(k)} \tag{22}$$

where

$$A_{w_{6\times6}} = \begin{bmatrix} A_w^{11} & A_w^{21} \\ I_{3\times3} & 0_{3\times3} \end{bmatrix} \tag{23}$$

$$A_w^{11} = \begin{bmatrix} -2\zeta_x w_x & 0 & 0 \\ 0 & -2\zeta_y w_y & 0 \\ 0 & 0 & -2\zeta_\psi w_\psi \end{bmatrix} A_w^{21} = \begin{bmatrix} -w_x^2 & 0 & 0 \\ 0 & -w_y^2 & 0 \\ 0 & 0 & -w_\psi^2 \end{bmatrix} \tag{24}$$

$$C_{21_{6\times6}} = C_{22_{6\times6}} = \begin{bmatrix} 1 & 0 & 0 & 0 & 0 & 0 \\ 0 & 1 & 0 & 0 & 0 & 0 \\ 0 & 0 & 0 & 0 & 0 & 0 \\ 0 & 0 & 0 & 0 & 0 & 0 \\ 0 & 0 & 0 & 0 & 0 & 0 \\ 0 & 0 & 0 & 0 & 0 & 1 \end{bmatrix} \tag{25}$$

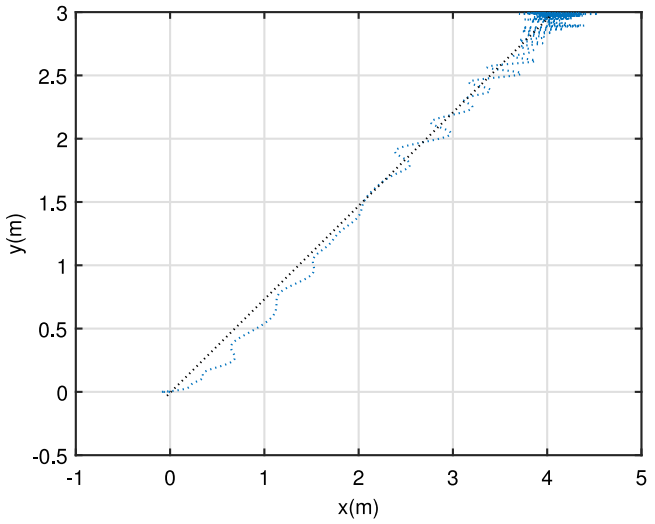

Fig. 8. 3GDL UKF control results with waves, position (x, y).

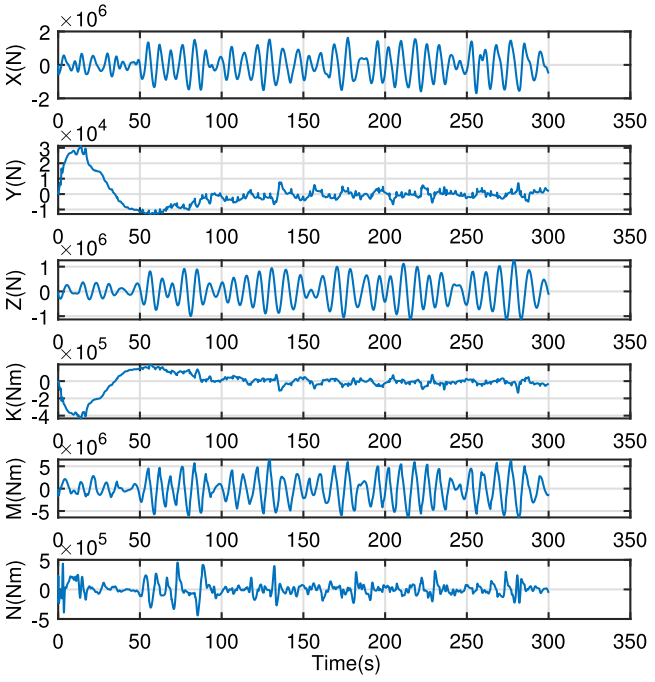

Fig. 9. 3GDL UKF control results with waves, forces and moments induced in the center of gravity of the caisson.

where $\zeta_i (i = x, y, \psi)$ are the wave relative damping ratio for each degree of freedom and $w_i (i = x, y, \psi)$ are the wave natural frequencies for each degree of freedom. $x_{w(k)} = [\eta^T_{w(k)}, \zeta^T_{w(k)}]^T$ is a measurement vector of the 1st order wave effects in surge, sway and yaw; where $\zeta^T_w = [\zeta_x, \zeta_y, \zeta_\psi]$ is a vector of internal states of the waves and $\eta^T_w = [w_x, w_y, w_\psi]$. $g_{(k)}(z_{c(k)}, F_{a(k)})$ is a discrete function of the non linear model defined in (1) which gives as a result a vector of 12 components $([0, 0, 0, 0, 0, 0, z_{c(k)}]^T)$, $y_{f(k)} = [y_{fx(k)}, y_{fy(k)}, y_{f\psi(k)}]^T$ are the outputs of the model, $w_{(k)} \sim N(0, Q)$ is the process noise vector and $n_{(k)} \sim N(0, R)$ is the measurement noise vector. $k \in \mathbb{N}$, and $\mathbb{N}$ is the set of natural numbers. The sub-index k, is assigned to a continuous time instant $t_{(k)}$.

In this way, the UKF filter uses a wave model of matrices (23) and (24), which facilitates the estimation of the low frequency components and the wave frequency components of the position $(x(k), y(k))$ and the

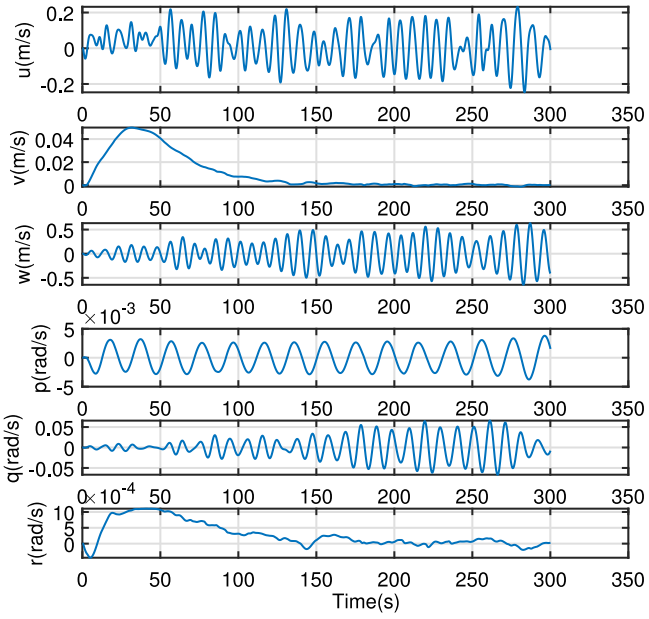

Fig. 10. 3GDL UKF control results with waves, speeds and angular speeds in the center of gravity of the caisson.

heading $(\psi(k))$ measurements. Note that the second order wave effects are not estimated with the UKF filter, the integral term of the controller designed in the next section will compensate those effects.

The UKF uses the so-called unscented transformation. That is, if we have the random variable $x_f = [x_w, z_c]^T$ and a static mapping $y_f = h(x_f)$) as previously indicated, one can specifically choose $2N + 1$ points χ_i (called sigma points) and weighting coefficients W_i, such that the weighted sample mean and covariance obtained from these points approximate the mean and covariance of x_f, that is $(\bar{x}_f, P_{x_f})$. Then, we can transform the sigma points using $h(\cdot)$ to obtain a set of sigma points for y_f, and estimate the mean and covariance of y_f, namely, $(\bar{y}_f, P_{y_f})$ using the weighted averages of the transformed sigma points. In order to do this, the matrix χ is made up by $2L + 1$ sigma vectors χ_i with their corresponding weights W_i in the following way:

$$\begin{aligned}
\chi_0 &= \bar{x}_f \\
\chi_i &= \bar{x}_f + (\sqrt{(L+\lambda)P_{x_f}})_i \quad i = 1, \ldots, L \\
\chi_i &= \bar{x}_f - (\sqrt{(L+\lambda)P_{x_f}})_{i-L} \quad i = L+1, \ldots, 2L \\
W_0^{(m)} &= \lambda/(L+\lambda) \\
W_0^{(c)} &= \lambda/(L+\lambda) + (1 - \alpha^2 + \beta) \\
W_i^{(m)} &= W_i^c = 1/(2(L+\lambda)) \quad i = 1, \ldots, 2L
\end{aligned} \tag{26}$$

where $\lambda = \alpha^2(L + \kappa) - L$ is a scaling parameter, α determines the spread of sigma points around the mean $\bar{x}_f$ (normally a small positive value 1e-3), L is the dimension of x_f, P_{x_f} is the covariance of x_f, κ is a secondary scaling parameter and β, it is used to incorporate prior knowledge of the x_f distribution (for Gaussian distributions, $\beta = 2$ is optimal).

The standard UKF algorithm is developed through the following steps:

1. Initialize the mean and covariance by:

$$\begin{aligned}
\hat{x}_{f(0)} &= E[x_{f(0)}] \\
P_{(0)} &= E[(x_{f(0)} - \hat{x}_{f(0)})(x_{f(0)} - \hat{x}_{f(0)})^T] \\
\hat{x}^a_{f(0)} &= E[x^a] = [\hat{x}^T_{f(0)} \; 0 \; 0]^T \\
P^a_{(0)} &= E[(x^a_{(0)} - \hat{x}^a_0)(x^a_{(0)} - \hat{x}^a_{(0)})^T] = \begin{bmatrix} P_0 & 0 & 0 \\ 0 & P_w & 0 \\ 0 & 0 & P_n \end{bmatrix}
\end{aligned} \tag{27}$$

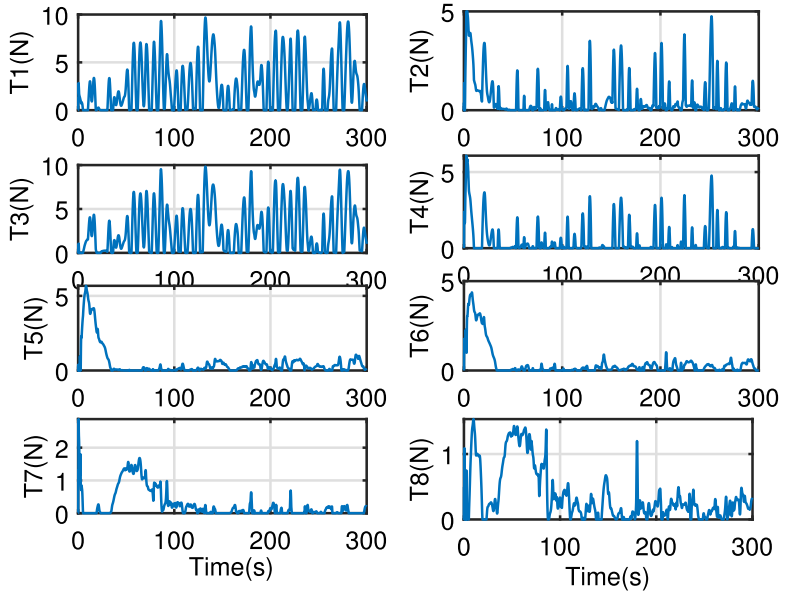

Fig. 11. 3GDL UKF control results with waves, tensions applied in each of the winches.

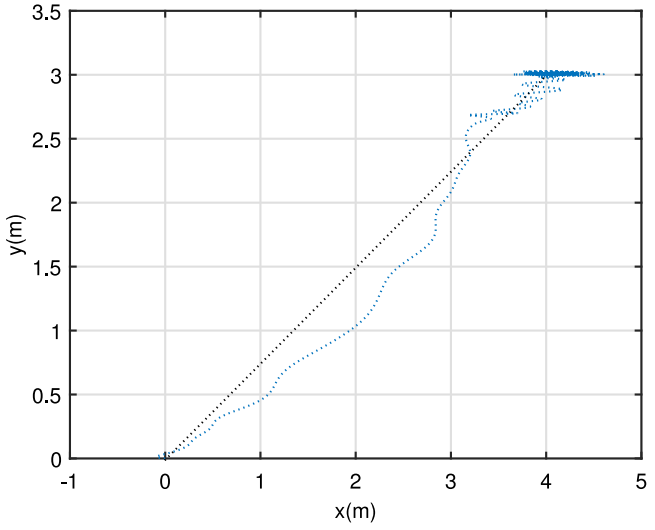

Fig. 12. 3GDL control results with waves, position (x, y).

For $k \in \{1, \ldots, \infty\}$

2. Establish a set of sigma points $\chi^{a}_{(k-1)}$ and weights W_{k-1} applying the Eqs. (26).
3. Propagate the transformed points through the process model

$$\chi^{x_f}_{(k|k-1)} = f(\chi^{x_f}_{(k-1)}, \chi^{v}_{(k-1)}, F_a(k), k) \tag{28}$$

4. Estimate the mean of the states, based on the weights and the propagated sigma points,

$$\hat{x_{f}}_{(k|k-1)} = \sum_{i=0}^{2L} W_i^{(m)} \chi^{x_f}_{(i,k|k-1)} \tag{29}$$

5. Estimate the covariance of the states,

$$P_{(k|k-1)} = \sum_{i=0}^{2L} W_i^{(c)} [\chi^{x_f}_{(i,k|k-1)} - \hat{x}_{f(k|k-1)}] \cdot [\chi^{x}_{(i,k|k-1)} - \hat{x}_{f(k|k-1)}]^T + Q \tag{30}$$

6. Transform the sigma points through output equations for the measurement sigma points

$$Y_{(k|k-1)} = h(\chi^{x_f}_{(k-1)}, \chi^{n}_{(k-1)}) \tag{31}$$

7. Estimate the mean of the measurements prediction,

$$\hat{y}_{f(k|k-1)} = \sum_{i=0}^{2L} W_i^{(m)} Y_{(i,k|k-1)} \tag{32}$$

8. Calculate the covariance,

$$P_{y_{f(k|k-1)}} = \sum_{i=0}^{2L} W_i^{(c)} [Y_{(i,k|k-1)} - \hat{y}_{f(k|k-1)}] \cdot [Y_{(i,k|k-1)} - \hat{y}_{f(k|k-1)}]^T + R \tag{33}$$

$$P_{xy_{(k|k-1)}} = \sum_{i=0}^{2L} W_i^{(c)} [\chi_{(i,k|k-1)} - \hat{x}_{f(k|k-1)}] \cdot [Y_{(i,k|k-1)} - \hat{y}_{f(k|k-1)}]^T \tag{34}$$

9. Update the estimates of the states and the covariance using new measurements,

$$\begin{aligned} K_{(k)} &= P_{xy_{(k|k-1)}} P^{-1}_{(y_{(k|k-1)})} \\ \hat{x}_{f(k)} &= \hat{x}_{f(k|k-1)} + K_{(k)}(y_{f(k)} - \hat{y}_{f(k|k-1)}) \\ P_{(k)} &= P_{(k|k-1)} - K_{(k)} P_{y_{f(k|k-1)}} K^T_{(k)} \end{aligned} \tag{35}$$

where, $x^a = [x_f^T w^T n^T]^T$, $\chi^a = [(\chi^{x_f})^T (\chi^w)^T (\chi^n)^T]^T$, W_i are the weights calculated in (26), Q is the covariance matrix of the process noise and R is the measurement noise covariance matrix.

In the implementation of the UKF, the Cholesky factorization (Press et al., 1992) is used in order to calculate the square root of the covariance matrix because it provides numerical stability and efficiency. The tuning of the UKF is done through the entries of the state and measurement noise, using the same criterion as with the standard Kalman filter tuning (Fossen and Perez, 2009). That is, if we believe the model is accurate, we lower the covariance of the state noise, which reduces the influence of noise on the estimates. However, if the model is believed to be uncertain, we need to increase the state covariance so the filter uses innovations $(y_{f(k)} - \hat{y}_{f(k|k-1)})$ to correct the predictions made with the uncertain model this reduces bias and increase noise in the estimates.

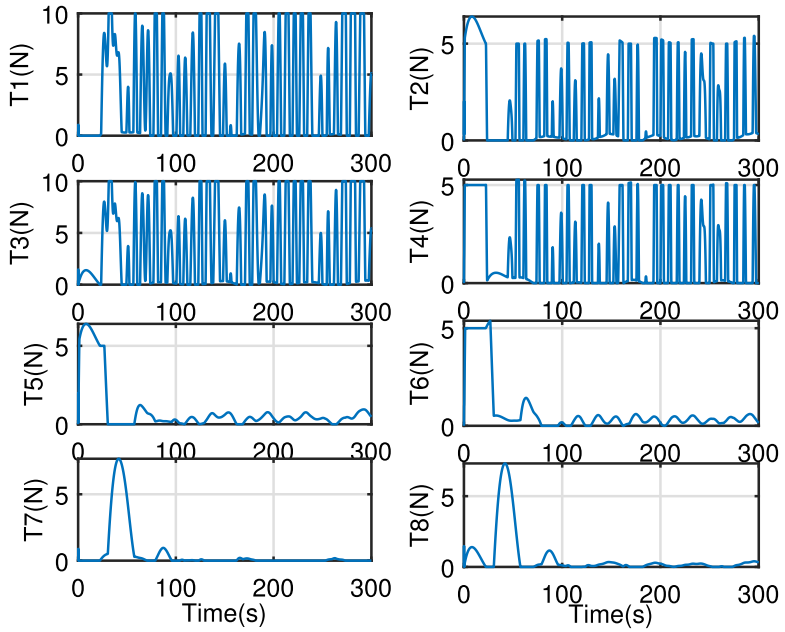

Fig. 13. 3GDL control results with waves, tensions applied in each of the winches.

The covariance matrix R of the UKF is due to sensors noise, which is uncorrelated, then R is chosen diagonal,

$$R = diag(\sigma_1^2,\ \sigma_2^2, \ldots, \sigma_{n_v}^2) \tag{36}$$

where, σ_i^2 is the measurement noise covariance of the measured variable i and n_v is the number of variables. $n_v = 3$ for the model indicated in (22). The states covariance matrix Q of the UKF, is also chosen diagonal,

$$Q = diag(Q_1,\ Q_2, \ldots,\ Q_{n_s}) \tag{37}$$

where Q_i is the state covariance of the variable i and n_s is the number of states. $n_s = 12$ for the model indicated in (21). The values of the Q matrix are chosen, assuming that the uncertainty is small, since the model of (1) is accurate.

4. The controller

In this section, we propose a three degrees of freedom controller based in classical methods for the loop indicated in Fig. 1, which generates a control vector of forces and moments, $F_c(t) = [X_c, Y_c, N_c]$ in order to follow a reference vector $ref(t) = [x_{ref}, y_{ref}, \psi_{ref}]$. Fig. 2 shows the structure of the dual loop controller for the surge degree of freedom, which includes an integral term for decreasing errors due to external disturbances and a lead compensation term in order to provide stability to the caisson behavior. The same control structure is applied for the rest degrees of freedom to be controlled: sway and yaw. It must be noted that the reference is applied through a first order system so that smooth motion of the caisson can be assured, this improve the safety of the operation which is part of the aim of this paper as commented before.

Since the design of the indicated controller is based on classical linear theory, we obtain an approximated linear model of the non linear one defined in Eq. (1). The approximated model is a set of transfers functions of the degrees of freedom to be controlled: surge, sway and yaw. The transfer function parameters were estimated using least squares with individual trails. Note that aim of the approximated model is just to the design the controller, which it is applied to the non linear model defined in Eq. (1).

The Laplace transfer function of the approximated model and the controller for each degree of freedom are found in Table 1. By means of the root locus theory the lead compensation controller indicated in Fig. 2 is designed.

5. Control allocation

The actuators of the DP system indicated in Fig. 1 are made up of eight anchor lines, see Appendix A for details relative to the lines configuration. Therefore, the actuators system is over-actuated since only three degrees of freedom are controlled: surge, sway and yaw. This makes the actuators system redundant as it is well known. Moreover, it must be noted that the mooring lines distribution of this work (see Fig. 15) provokes coupling among the different axes of the coordinate system fixed to the center of gravity, which means that the corrections made in one of the degrees of freedom to control its motion have an impact in the rest of them. Additionally, the forces induced in the caisson by the different mooring lines are not constant and vary with the relative position and attitude of the eyebolts distributed on the top of the caisson with respect to the anchor points in the seabed.

In this section, it is established how the control forces and moments $Fc(t) = [X_c, Y_c, N_c]$ generated by the controller are equally distributed over the anchor lines by generating a vector of tensions $T(t) = [T_1, T_2, T_3, T_4, T_5, T_6, T_7, T_8]^T$. The developed control allocation module is presented in Algorithm 1, which matrices are defined in Eq. (38). This algorithm has the advantage that is easy to implement and computationally cheap.

$$A_1 = \begin{bmatrix} 0&0&0\\ 1&0&0\\ 0&0&0\\ 1&0&0\\ 0&0&0\\ 0&0&0\\ 0&0&0\\ 0&0&0 \end{bmatrix} A_2 = \begin{bmatrix} 1&0&0\\ 0&0&0\\ 1&0&0\\ 0&0&0\\ 0&0&0\\ 0&0&0\\ 0&0&0\\ 0&0&0 \end{bmatrix} A_3 = \begin{bmatrix} 0&0&0\\ 0&0&0\\ 0&0&0\\ 0&0&0\\ 0&1&0\\ 0&1&0\\ 0&0&0\\ 0&0&0 \end{bmatrix}$$

$$A_4 = \begin{bmatrix} 0&0&0\\ 0&0&0\\ 0&0&0\\ 0&0&0\\ 0&0&0\\ 0&0&0\\ 0&1&0\\ 0&1&0 \end{bmatrix} A_5 = \begin{bmatrix} 0&0&0\\ 0&0&1\\ 0&0&1\\ 0&0&0\\ 0&0&1\\ 0&0&0\\ 0&1&0\\ 0&1&1 \end{bmatrix} A_6 = \begin{bmatrix} 0&0&1\\ 0&0&0\\ 0&0&0\\ 0&0&1\\ 0&0&0\\ 0&0&1\\ 0&1&1\\ 0&1&0 \end{bmatrix} \tag{38}$$

Algorithm 1: Control allocation module.

Initialize $T_{max} = 10$ and $n_l = 8$;
Load the control signals $[X, Y, N]$;
for k $(\in 1, \ldots, \infty)$ **do**
  if $X > 0$ **then**
    $f_{12} = A_1$;
  else
    if $X < 0$ **then**
      $f_{12} = A_2$;
    end if
  end if
  if $Y > 0$ **then**
    $f_{34} = A_3$;
  else
    if $Y < 0$ **then**
      $f_{34} = A_4$;
    end if
  end if
  if $N > 0$ **then**
    $f_{56} = A_5$;
  else
    if $N < 0$ **then**
      $f_{56} = A_6$;
    end if
  end if
  Add the contributions of all of the axis $S = [f12 + f34 + f56]^T$;
  Adjust the gain $S = S/2$;
  Calculate the tensions of the n_l lines $T = S * abs([y_{fX}, y_{fY}, y_{fN}])$;
  for j $(\in 1, \ldots, n_l)$ **do**
    if $T(j) > T_{max}$ **then**
      $T(j) = T_{max}$;
    end if
  end
end
T_{max} maximum value of the tension, n_l number of anchor lines.

6. Simulation results

The simulations of this section follow the logic and rationale as the theory previously presented in this article: including the non linear hydrodynamical model, the dual loop controller, the UKF filter and the control allocation. For the evaluation of the proposed control scheme for DP system (Fig. 1), we simulate a case of study for the caisson indicated in Appendix A under external perturbances induced by waves. The simulations here presented were run in Matlab and a time step of 0.1s was used. The simulation scheme followed in this article is sum up as follows:

- Based on the theory presented in Section 4, the controller is designed by root locus analysis.
- The DP control scheme of Fig. 1 with the controller previously designed is implemented. The statistical properties and the performance of the UKF filter are verified. The simulations are run to establish a comparison between the DP control scheme with a first order network filter and with the UKF filter.

The next subsections develops these bullet points.

6.1. Controller design simulations

Fig. 3 depicts an analysis, which compares the root locus of the linear approximation (top of the figure) to the one with the inclusion of the lead compensation controller (bottom of the figure). As far as the surge and sway degrees of freedom are concern, their root locus branches are on the imaginary axis, which may produce unstable behavior. However, when the lead compensation controller is introduced in the system, the branches are out of the imaginary axis and tends to a break-in point. This is due to the criteria established for the position of the poles and the zeros of the controller, see Table 1. This means that for positive values of the lead compensation controller gain $K_i (i = x, y, \psi)$, the behavior of the caisson is going to be stable, this values are chosen based on previous knowledge of the caisson dynamics. It must be noted that for dimensions of the caisson, the forces and moments due to caisson motion are high and therefore the gain values $K_i (i = x, y, \psi)$ are high too.

GOBIERNO DE ESPAÑA MINISTERIO DE CIENCIA E INNOVACIÓN AGENCIA ESTATAL DE INVESTIGACIÓN

Fig. 14. Spanish FEDER/Ministry of Science, Innovation and Universities — State Research Agency.

6.2. DP simulations

The reference vector was set to $ref = [x_{ref}, y_{ref}, \psi_{ref}] = [4, 3, 5]$, the UKF matrices were tuned by doing $Q = 10^{-4} I_{12}, R = 0.04 I_3, P = 0.001 I_{12}$. The wave parameters used were: height of 1 m, a period of 8 s and direction of 0 degrees in x axis. Fig. 5 depicts the wave forces and moments induced to the caisson with the cited wave parameters.

Fig. 4 shows the statistical properties of the UKF filter by drawing the histogram of the residuals for the surge, sway and yaw degrees of freedom. The histogram is drawn following the expression (Lloyd, 1998):

$$f = N_h/(NW_h) \tag{39}$$

where N_h is the number of measurements of the bar, W_h is the width of the bar and N is the total number of measurements. Next, the corresponding Gaussian probability distribution is drawn over the histogram to check if the parameter distribution is Gaussian or normal. Fig. 4 exhibits a normal distribution of the residuals, which confirms that it is possible to apply the UKF filter to the application proposed on this work.

Figs. 6 to 11 present the results of the proposed control scheme. It is shown how the system is able to compensate the second order wave effects thanks to the integral term added in the dual loop as shown in Fig. 2, since the system is able to follow the reference with no stationary state error (see Fig. 7). Moreover, the UKF is able to filter the first order wave effects as can be seen in Fig. 7, see the zoomed part of the figure for the surge degree of freedom where the waves provoke a higher incidence in the caisson motion. The results of the system in the x-plane, y-plane indicate a low oscillation despite the disturbances (see Fig. 8) when controlling the caisson from a starting point to a final point as indicated in Fig. 6.

Additionally, simulations have been carried out with the same controller and disturbances as in the previous case but using a first order network as a filter. Comparing the results obtained in Fig. 8 with the UKF to those of Fig. 12 with the first order network, a higher deviation can be appreciated in the path described by the caisson with respect to the reference path (a line between the initial and final point) when the first order network is used. Moreover, if Fig. 11 is compared with Fig. 13, a greater control effort is observed when applying the first order network as a filter, due to the abruptly changes and saturations that occur in the tensions applied to some of the lines. This means that the inclusion of the UKF filter increases the safety of the operation and the life expectancy of the actuators, which constitutes one of the aims of this work.

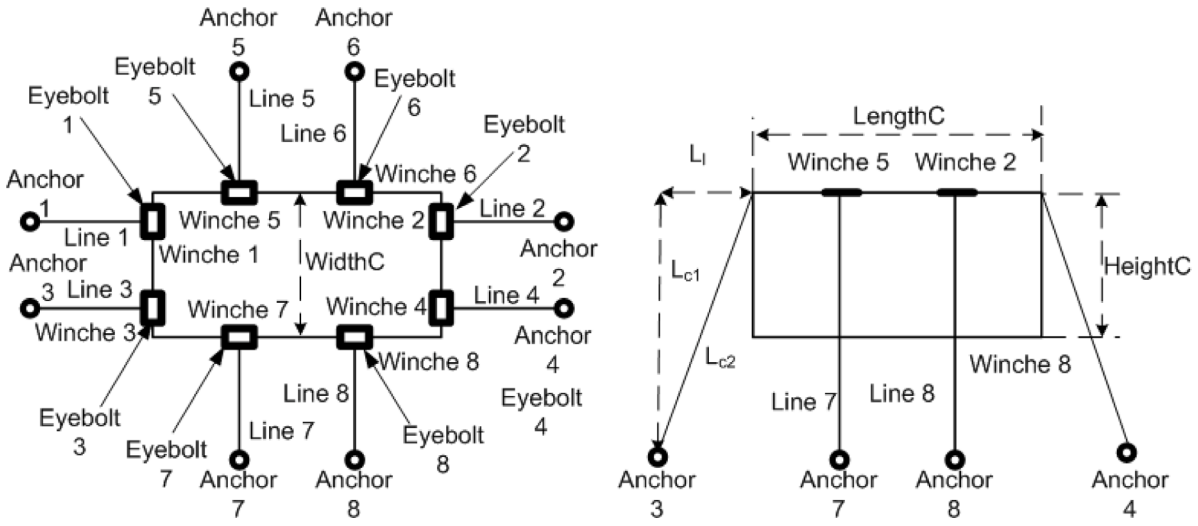

Fig. 15. Mooring lines distribution of the caisson (left plant view, right lateral view).

7. Conclusions and further research

In this paper, we propose a control scheme, which includes a dual loop controller, a non linear filter based on the UKF and a control allocation system for DP operations. The simulations were performed to verify the effectiveness of the approach. The results show no error in stationary states thanks to the integral term added in the dual loop controller, which is able to compensate second order wave effects. Moreover, the low oscillation in the caisson's trajectory means that the controller compensate first order wave effects too. Finally, it is compared the results given by the dual loop controller with a first order network to the ones given by the dual loop controller with the UKF. We conclude that the controller with the UKF provides a reduction in the deviation from the reference path and also a reduction in the control effort. Therefore, a longer life expectancy of the actuators and an improvement in safety of the operation is expected. In subsequent research, an in-scale model a caisson is going to be developed in order to perform trials in a model basin with the implementation of the control scheme proposed in this article.

CRediT authorship contribution statement

Elías Revestido Herrero: Methodology, Investigation, Writing - original draft. **Jose Ramon Llata:** Methodology, Investigation. **Esther Gonzalez-Sarabia:** Validation. **Francisco J. Velasco:** Supervision. **Jose Joaquin Sainz:** Software. **Alvaro Rodriguez-Luis:** Software. **Sergio Fernandez-Ruano:** Software. **Raul Guanche:** Supervision.

Declaration of competing interest

No author associated with this paper has disclosed any potential or pertinent conflicts which may be perceived to have impending conflict with this work. For full disclosure statements refer to https://doi.org/10.1016/j.oceaneng.2021.109055.

Acknowledgments

The Spanish FEDER/Ministry of Science, Innovation and Universities — State Research Agency (Fig. 14) is greatly acknowledged for funding our research through SAFE Project (Desarrollo de un Sistema Autónomo para el Fondeo de Estructuras para Obras Marítimas), Grant Agreement: RTC-2017-6603-4.

The authors would like to thank FCC CO as a collaborator in the development of the SAFE Project.

R. Guanche also acknowledges financial support from the Ramon y Cajal Program (RYC-2017-23260) of the Spanish Ministry of Science, Innovation and Universities.

Appendix A. Caisson main features

The caisson is shown in figure and its lines distribution in Fig. 15. The main data of the caisson including the moments of inertia, the center of gravity and center of buoyancy are found in Table 2.

References

Aamo, O.M., Fossen, T.I., 1999. Controlling line tension in thruster assisted mooring systems. In: Proceedings of the 1999 IEEE International Conference on Control Applications (Cat. No.99CH36328), Vol. 2, pp. 1104–1109.

Aamo, O.M., Fossen, T.I., 2001. Finite element modelling of moored vessels. Math. Comput. Model. Dyn. Syst. 7 (1), 47–75. http://dx.doi.org/10.1076/mcmd.7.1.47.3632, http://arxiv.org/abs/https://www.tandfonline.com/doi/pdf/10.1076/mcmd.7.1.47.3632, https://www.tandfonline.com/doi/abs/10.1076/mcmd.7.1.47.3632.

Armesto, J.A., Guanche, R., Jesus, F.d., Iturrioz, A., Losada, I.J., 2015. Comparative analysis of the methods to compute the radiation term in cummins' equation. J. Ocean Eng. Mar. Energy 1 (4), 377–393. http://dx.doi.org/10.1007/s40722-015-0027-1.

Berntsen, P.I.B., Aamo, O.M., L., B.J., Sorensen, A.J., 2008. Structural reliability-based control of moored interconnected structures. Control Eng. Pract. 16 (4), 495–504. http://dx.doi.org/10.1016/j.conengprac.2006.03.004, http://www.sciencedirect.com/science/article/pii/S0967066106000761, Special Section on Manoeuvering and Control of Marine Craft.

Cejuela, E., Negro, V., Del Campo, J.M.a., Martín-Antn, M., Esteban, M.D., Lpez-Gutirrez, J.S., 2018. Recent history, types, and future of modern caisson technology: The way to more sustainable practices. Sustainability 10 (11), http://dx.doi.org/10.3390/su10113839, https://www.mdpi.com/2071-1050/10/11/3839.

Chen, M., Ge, S.S., How, B.V.E., Choo, Y.S., 2013. Robust adaptive position mooring control for marine vessels. IEEE Trans. Control Syst. Technol. 21 (2), 395–409.

Chen, Y., Yang, X., Liu, R., 2018. A nonlinear sate estimate for dynamic positioning based on improved particle filter. In: 2018 2nd IEEE Advanced Information Management, Communicates, Electronic and Automation Control Conference (IMCEC), pp. 880–884.

Cheng-Du, Z., Xi-Huai, W., Jian-Mei, X., 2013. Ship dynamic positioning system based on backstepping control. J. Theor. Appl. Inf. Technol. 51 (1), 129–136.

Fang, M.-C., Lee, Z.-Y., 2016. Application of neuro-fuzzy algorithm to portable dynamic positioning control system for ships. Int. J. Nav. Archit. Ocean. Eng. 8 (1), 38–52. http://dx.doi.org/10.1016/j.ijnaoe.2015.09.003.

Fossen, T.I., Johansen, T.A., 2006. A survey of control allocation methods for ships and underwater vehicles. In: Proceedings of the 14th Mediterranean Conference on Control and Automation, Piscataway, NJ, USA, p. 6.

Fossen, T.I., Perez, T., 2009. Kalman filtering for positioning and heading control of ships and offshore rigs. IEEE Control Syst. Mag. 29 (6), 32–46.

Jayasiri, A., Nandan, A., Imtiaz, S., Spencer, D., Islam, S., Ahmed, S., 2017. Dynamic positioning of vessels using a UKF-based observer and an NMPC-based controller. IEEE Trans. Autom. Sci. Eng. 14 (4), 1778–1785.

Johansen, T.A., Fossen, T.I., 2013. Control allocationa survey. Automatica 49 (5), 1087–1103. http://dx.doi.org/10.1016/j.automatica.2013.01.035, http://www.sciencedirect.com/science/article/pii/S0005109813000368.

Journee, L.M., 2001. Offshore Hydromechanics. Delft: Delft University of Technology.

Julier, S.J., Uhlmann, J.K., 1997. A new extension of the Kalman filter to nonlinear systems. In: Aerosense: 11th Int. Symp. on Aerospace Defence Sensing, Simulation and Control.

Lloyd, A., 1998. SEAKEEPING: Ship Behaviour in Rough Weather.

Press, W.H., Teukolsky, S.A., Vetterling, W.T., Flannery, B.P., 1992. Numerical Recipes in C: The Art of Scientific Computing, second ed. Cambrige University Press.

Ristic, B., Arulampalam, S., Gordon, N., 2004. Beyond the Kalman Filter. Artech House.

Sorensen, A.J., 2011. A survey of dynamic positioning control systems. Annu. Rev. Control 35 (1), 123–136.

Sorenson, H.W., 1985. Kalman Filtering: Theory and Application. IEEE Press.

Uhlmann, J.K., 1992. Algorithms for multiple target tracking. Am. Sci. 80 (2), 128–141.

Xia, G., Xue, J., Jiao, J., 2018. Dynamic positioning control system with input time-delay using fuzzy approximation approach. Int. J. Fuzzy Syst. 20 (2), 630–639. http://dx.doi.org/10.1007/s40815-017-0372-4.

Xia, G., Xue, J., Sun, C., Zhao, B., 2019. Backstepping control using barrier Lyapunov function for dynamic positioning control system with passive observer. Math. Probl. Eng. 2019, http://dx.doi.org/10.1155/2019/8709369, 8709369 (9 pp.).

Xu, D., Du, J., Hu, X., Li, H., 2014. Sliding mode observer design for ship dynamic positioning systems. In: Fifth International Conference on Intelligent Control and Information Processing (ICICIP). Proceedings, Piscataway, NJ, USA. pp. 151–154. http://dx.doi.org/10.1109/ICICIP.2014.7010330, ship dynamic positioning systems; state estimation; unknown external disturbances; sliding mode observer structural principle; global asymptotic stability.

Xu, L., Liu, Z., 2016. Design of fuzzy PID controller for ship dynamic positioning. In: 2016 Chinese Control and Decision Conference (CCDC), pp. 3130–3135.

Xu, L., Xu, H., Feng, H., Li, W., Bu, D., Song, X., 2013. Estimation of low-frequency motion for ship dynamic positioning. In: 2013 Ninth International Conference on Natural Computation (ICNC), pp. 1655–1659.

Zhao, D., Gao, S., Spurgeon, S.K., Reichhartinger, M., 2019. Adaptive sliding mode dynamic positioning control for a semi-submersible offshore platform. In: 2019 18th European Control Conference (ECC), Piscataway, NJ, USA. pp. 3103–3108. http://dx.doi.org/10.23919/ECC.2019.8796093.